JOURNAL OF MATERIALS SCIENCE 24 (1989) 1327–1331

Oxide scale stresses in polycrystalline Ni200

N. JAYARAMAN
Department of Materials Science and Engineering, University of Cincinnati, Cincinnati, Ohio 45221-0012, USA

MICHAEL J. VERRILLI
Fatigue and Fracture Section, NASA Lewis Research Center, Cleveland, Ohio 44135, USA

An X-ray diffraction ($\sin^2\psi$) method has been successfully used to measure the oxidation stresses at room temperature in annealed and electropolished samples of polycrystalline Ni200 coupons oxidized in the temperature range 760 to 982° C for 4 h. The stresses on the free surface of the oxide (σ_{11} and σ_{22}) were compressive and the average stress through the thickness ($\hat{\sigma}_{33}$) normal to the oxide layer was found to be tensile. Surface stresses on the oxides formed at temperatures up to 927° C were found to be isotropic and both surface stresses and the average normal stress increased with increasing temperature of oxidation. At 982° C, the surface stresses were lower and this was attributed to the deformation and fracture of oxide layer resulting in stress relaxation.

1. Introduction

Generation of stresses in the oxide layer and the metal substrate during oxidation of metals was recognized long ago by Pilling and Bedworth [1]. Subsequent research in this area was primarily devoted to understanding the mechanisms responsible for such stresses and in demonstrating its presence qualitatively and semi-quantitatively. This subject has been the topic of two conferences [2, 3] and reviewed by several researchers [4–9].

2. Origin of stresses in oxide scales

A number of factors have been identified to contribute towards generation of stresses in oxide scales. Some of them are: (i) volume difference between the oxide formed and the metal consumed (the Pilling–Bedworth ratio) during oxidation; (ii) macroscopic and microscopic curvature in the samples; (iii) concentration gradients of defects and changes in stoichiometry through the thickness of the oxide scale; (iv) epitaxial constraints, if the oxide layer is thin; (v) differences in thermal expansion characteristics between the oxide layer and the metal substrate. The effects of these different factors have been well discussed by Stringer [5] and Cathcart and Pawel [9]. Experimentally it is difficult to distinguish the contribution due to the different factors mentioned above. However, a knowledge of the overall stress state in the oxide layer, regardless of the origin, is of great fundamental interest from the standpoint that it could possibly control the integrity of the oxide scale. In this regard, development of experimental techniques for reliable measurement of stresses in oxide scales is important. Pawel and co-workers [10–12] developed a flexure technique and use it for measuring oxidation stresses in some refractory metal–metal oxide systems. Hancock and co-workers [13–16] developed a vibration technique for studying a number of metal–metal oxide systems. In this paper, we present the results obtained from X-ray diffraction techniques on the oxide scale stresses in NiO grown on polycrystalline Ni200, nominal composition (wt %) 99.5% Ni, 0.08% C, 0.15% Mn, 0.15% Fe, 0.005% S, 0.05% Si and 0.05% Cu.

3. Experimental methods

3.1. Specimen preparation

Small blanks of Ni200 of dimensions 3.8 cm × 3.8 cm × 0.3 cm were cut from a large sheet. The blanks were cross-rolled at room temperature to a thickness of 0.5 mm by several passes. Experimental specimens of 4 cm × 4 cm were cut from the rolled sheet. One side of the specimens was mechanically polished down to 0.5 μm Al_2O_3 wet polishing wheel using standard metallographic techniques. These samples were then annealed at 982° C for 2 h under an atmosphere of a mixture of argon and hydrogen. The annealed samples were then electropolished and were tested for and found to have no residual stresses. The annealed samples were also tested on a Laue back-reflection apparatus and found to have no preferred orientation. Oxidation was carried out at 760, 816, 871, 927 and 982° C in dry oxygen gas atmosphere for 4 h, and the samples were cooled to room temperature in an inert atmosphere of pure argon.

3.2. X-ray diffraction

The experimental method was the conventional X-ray diffraction ($\sin^2\psi$) method [17]. A Philips–Norelco diffractometer, automated by a microcomputer, was used. A line source of copper radiation was used at the operating conditions of 40 kV and 20 mA. A nickel filter, a soller slit assembly and a 1/2° divergent slit were used on the incident beam side. A 1/2° receiving slit, a soller slit assembly and a graphite crystal diffracted beam monochromator were used on the diffracted beam side. The diffracted beam was detected by a

0022–2461/89 $03.00 + .12

scintillation detector. The diffractometer was calibrated periodically with the Si(3 1 1) diffraction beam from a standard powder sample. In addition, the diffractometer was calibrated with vacuum-annealed copper powder sample in the high-angle region using the Cu(4 2 0) peak at a Bragg angle, 2θ of 155.57° [18]. The ψ-angle was manually adjusted by using a specially designed sample holder which enables the sample to be rotated about the diffractometer axis in steps of 15°. The fact that the diffractometer axis coincided with the axis of rotation was confirmed by determining the position of the diffraction peak for Cu(4 2 0) for ψ-tilts varying from 0 to 60°. The observed variation in the Bragg angles for various ψ-tilts were well within the experimental scatter of 0.01° of 2θ. For the NiO layer formed on Ni200 substrate the (4 2 2) diffraction peak was examined at ψ-angles of 0, 15, 30, 45 and 60°. A strain-free NiO sample would produce a (4 2 2) peak at the Bragg angle of 129.202° of 2θ, corresponding to an interplanar spacing of 0.085 27 nm [18]. Because a diffracted beam monochromator was used, the receiving slit assembly was not moved radially to maintain focusing conditions. Other studies have shown that the results are essentially unaffected by this factor [19].

The procedure for determining the precise position of the diffracted beam consisted of step scanning by intervals of 0.01° with counting time of 40 or 80 sec at each step. This resulted usually in a peak-to-background ratio of 20 to 1 for annealed copper powder sample ((4 2 0) peak) and for annealed nickel sheet sample ((4 2 0) peak). For the NiO on the Ni200 substrate the counting time of 80 sec resulted in a peak to background ratio of 5 to 1. A parabolic curve-fitting to the data corresponding to the top 25% intensity range was done to determine the precise position of the peak.

4. Results and analysis

Analysis of the X-ray diffraction data was carried out according to the method suggested by Noyan [20]. The orthogonal co-ordinate system used in the analysis is exactly the same as that used by Noyan, and it is shown in Fig. 1. The specimen axes are defined such that S_1 and S_2 are in the surface of the sample. The diffraction is sampled in the laboratory system, and the direction L_3 defines the normal to the family of planes whose d spacings are being measured by X-rays. Direction L_2 is in the plane defined by S_1 and S_2 and makes an angle of ϕ with S_2. As per the method suggested by Noyan [20], the primed tensor quantities refer to the laboratory system L_1, and the unprimed tensor quantities to the sample system S_i. Accordingly, using the lattice spacing $d(4\,2\,2)_0$ of NiO from the literature

$$(\varepsilon'_{33})_{\phi,\psi} = \frac{[d(4\,2\,2)_{\phi,\psi} - d(4\,2\,2)_0]}{d(4\,2\,2)_0} \quad (1)$$

Noyan has shown that the stress state in the sample can be determined by using the $(\varepsilon'_{33})_{\phi,\psi}$–$\sin^2\psi$ data. The complexity of the analysis would depend upon the complexity of the actual stress state present in the material. One of the simplest cases, considered as a special case by Noyan, would be when the stress state on the free surface of the oxide scale is isotropic, resulting in stress tensor of the form

$$\sigma_{ij} = \begin{bmatrix} \sigma_{11} & \delta & \delta \\ \delta & \sigma_{11} & \delta \\ \delta & \delta & \hat{\sigma}_{33} \end{bmatrix} \quad (2)$$

where $\delta \ll \sigma_{ij}$. According to this special case, the slope and the intercept of the $(\varepsilon'_{33})_{\phi,\psi}$ against $\sin^2\psi$ plot would be independent of ϕ. The NiO layer on the Ni200 substrate under the present experimental conditions appears to have a stress state defined by the above type tensor. The experimental results, as will be shown later, tend to indicate that the slope and intercept of the (ε'_{33}) against $\sin^2\psi$ data have similar values for two different orientations of the samples $\phi = 0°$ and $\phi = 90°$ (ϕ is defined in Fig. 1).

Interplanar spacings for the (4 2 2) planes of NiO, $d(4\,2\,2)_{NiO}$, were calculated from the precise diffraction angles found as described in the previous section using a wavelength of $CuK\alpha_1 = 0.154\,0562$ nm [17]. (ε'_{33}) were calculated from Equation 1. A value of $d_0(4\,2\,2)_{NiO} = 0.085\,27$ nm for the stress-free NiO was obtained from [18]. The results are plotted as a function of $\sin^2\psi$ in Figs (a) to (e) for the oxidation temperatures 760, 816, 871, 927 and 982° C, respectively. Before beginning to interpret these results, we have to determine the average depth of penetration of X-rays, T, in the sample. This can be calculated for all the ψ-angles by using the relation suggested by Kelly and Short [21]

$$T = \frac{\sin\theta\cos\psi}{2\mu} \quad (3)$$

where θ is the Bragg angle and μ the linear absorption coefficient. A calculated value of $\mu = 277\,\text{cm}^{-1}$ for NiO was used, and from Equation 3, a T against $\sin^2\psi$ plot was obtained as shown in Fig. 3.

In Figs 2a to e, the depth of penetration of X-rays is a maximum for $\sin^2\psi = 0$ (or $\psi = 0°$) and it is a minimum for $\sin^2\psi = 0.75$ (or $\psi = 60°$). The data for any one oxidation temperature indicates that the

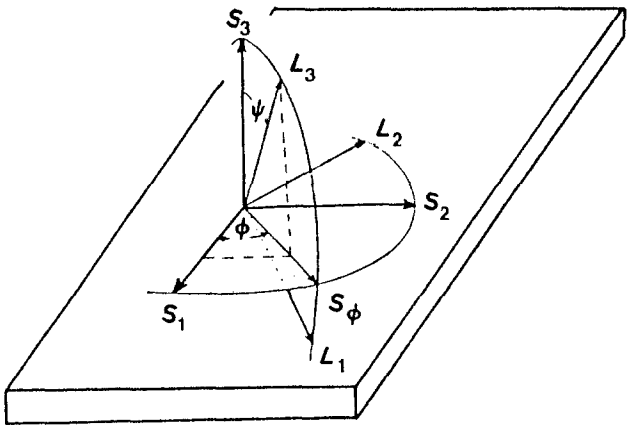

Figure 1 Geometry of sample and diffraction. The axes labelled S_1 are the specimen axes and L_1 are the laboratory axes. L_3 is the diffracting plane normal (from [20]). For a given specimen interplanar spacings were measured for angles $\psi = 0, 15, 30, 45$, and 60° and angles $\phi = 0$ and 90°.

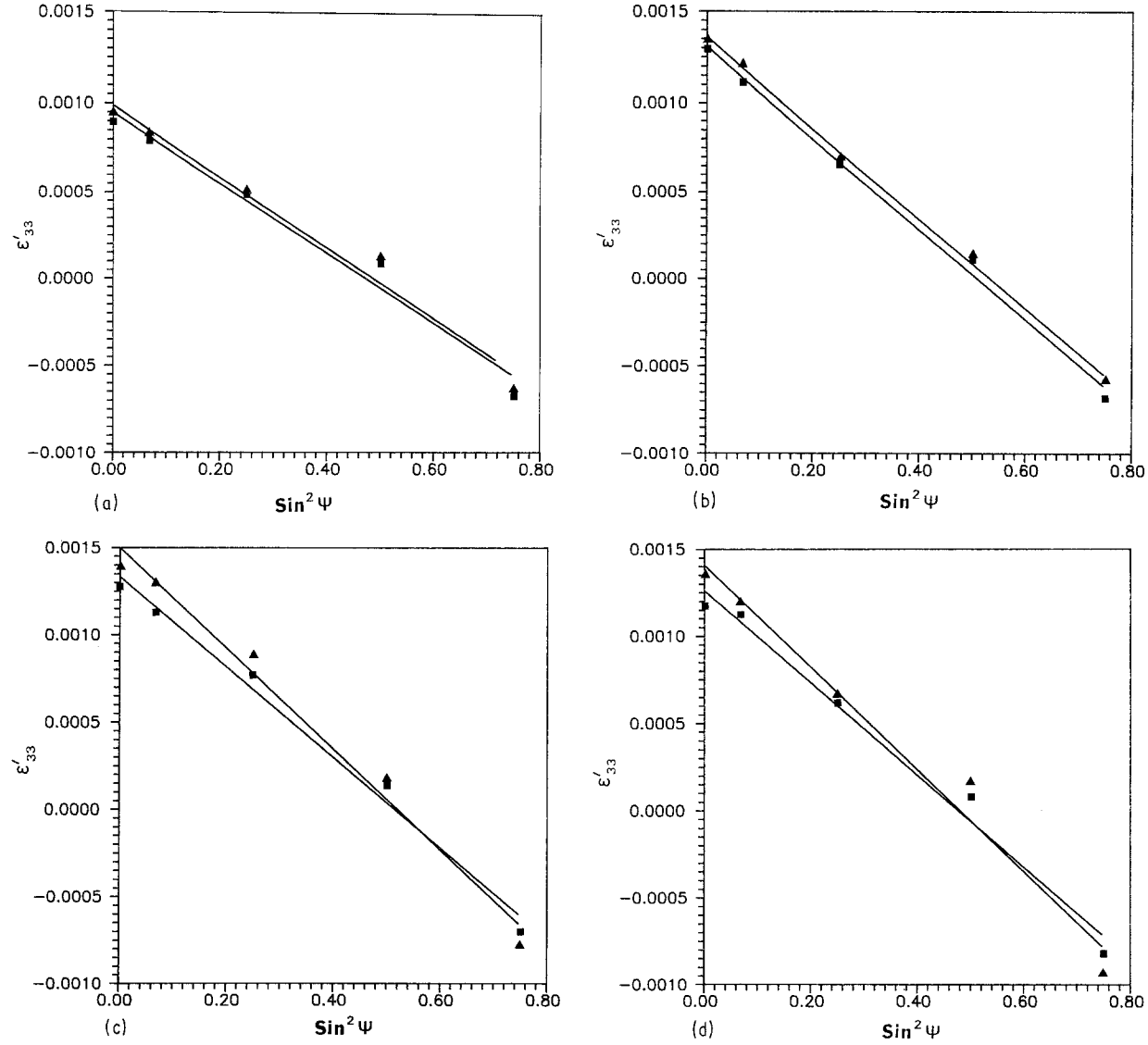

Figure 2 Plot of ε'_{33} against $\sin^2\psi$. All samples were oxidized for 4 h (■) $\phi = 0°$, (▲) $\phi = 90°$. Oxidation temperatures (a) 760, (b) 816, (c) 871, (d) 927 and (e) 982° C.

$d(4\,2\,2)_{NiO}$ is a maximum and larger than the value for stress-free NiO for $\sin^2\psi = 0$ and it is a minimum and smaller than the value for stress-free NiO for $\sin^2\psi = 0.75$. The variation of $d(4\,2\,2)_{NiO}$ as a function of $\sin^2\psi$ is slightly non-linear. The slope, intercept and the correlation coefficient for all the set of data are listed in Table I.

Rewriting Equation 14 of Noyan's paper [20]

$$\varepsilon'_{33} = \frac{(1+\nu)}{E}(\sigma_{11} - \hat{\sigma}_{33})\sin^2\psi + \frac{(1+\nu)}{E}\hat{\sigma}_{33} - \frac{\nu}{E}(\sigma_{33} + 2\sigma_{11}) \quad (4)$$

where ν is Poisson's ratio assumed to be 0.3 for NiO, E the elastic modulus, 1.11×10^5 MPa (16.1×10^6 psi) for NiO (from [22]), σ_{11} the stress on the surface of oxide scale in any direction lying on the surface, and $\hat{\sigma}_{33}$ the average stress in the direction normal to the surface.

Equation 4 is of the form $y = mx + c$, where the slope

$$m = \frac{(1+\nu)}{E}(\sigma_{11} - \hat{\sigma}_{33}) \quad (5)$$

and the intercept at $\psi = 0°$

$$c = \frac{(1+\nu)}{E}\hat{\sigma}_{33} - \frac{\nu}{E}(\hat{\sigma}_{33} + 2\sigma_{11}) \quad (6)$$

Values of m and c for the set of data points in Figs 2a to e were determined by least square methods. Now

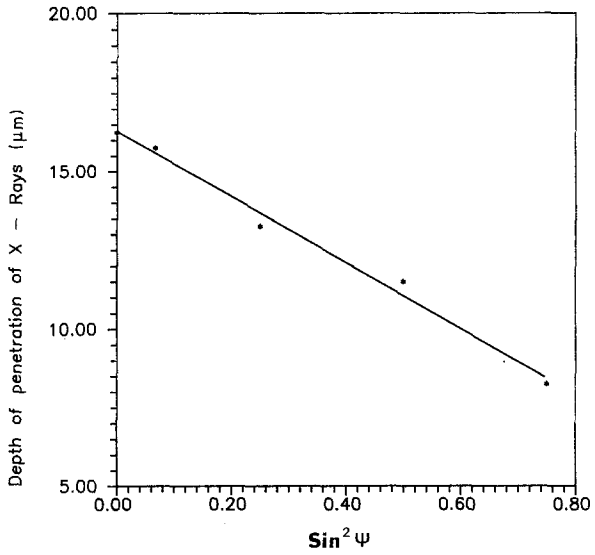

Figure 3 Plot of average depth of penetration of X-rays, T, against $\sin^2\psi$ for NiO.

Equations 5 and 6 can be solved simultaneously to yield the values of σ_{11} and $\hat{\sigma}_{33}$. These stress values are plotted against oxidation temperature in Fig. 4 and are also listed in Table II.

It is seen from Fig. 4 that the surface in-plane stress, σ_{11}, is compressive, and it increases with increasing temperature from about -160 MPa for oxidation at 760° C to about -235 MPa for oxidation at 927° C. However, the σ_{11} value drops to about -100 MPa for oxidation at 982° C. $\hat{\sigma}_{33}$, the average normal stress through the thickness, increases very slightly with increasing temperature of oxidation. Also, the difference in the stress values obtained for the two different ϕ-angles appear to be a minimum for all oxidation temperatures except 982° C.

These results should be analysed in conjunction with the microstructural observations. Figs 5a and b show scanning electron micrographs of typical surface regions on samples oxidized at 871 and 982° C, respectively. The oxide scale surface in Fig. 5a shows equiaxed grains of NiO formed at 871° C. However, at 982° C (Fig. 5b), the oxide scale appears to have "buckled" in several places. This buckling appears to be due to the combination of high inplane compressive stresses (σ_{11}) and high average normal stress ($\hat{\sigma}_{33}$). A typical buckled region is shown in Fig. 5b. The buckling of the oxide scales will result in considerable stress relaxation. Therefore the measured stresses on the scales formed at this temperature is much less than the corresponding values on scales formed at lower temperatures. Also, the buckling could explain the larger differences in the stress values between the two orientations found at this temperature. The above observations are consistent with the Rhines model for oxidation of nickel. For example, Rhines and Connell [23] report the "extrusion" of the oxide formed at 1000° C due to plastic deformation of the oxide scale, which we believe is the same as the buckling of the oxide scale that we have reported here.

TABLE I Slopes, intercepts and correlation coefficients for ε'_{33} vs $\sin^2\psi$ plots

Oxidation temperature, °C	ϕ	Slope ($\times 10^{-3}$)	Intercept ($\times 10^{-3}$)	Correlation coefficient
760	0	−2.02	0.95	0.9880
	90	−2.03	0.99	0.9893
816	0	−2.57	1.31	0.9975
	90	−2.55	1.36	0.9998
871	0	−2.59	1.33	0.9943
	90	−2.89	1.50	0.9920
927	0	−2.64	1.26	0.9928
	90	−2.92	1.41	0.9887
982	0	−2.28	1.27	0.9975
	90	−2.09	1.27	0.9983

Note: ε'_{33} is the average elastic strain measured from interplanar spacings of (4 2 2) NiO planes whose plane normals are inclined at an angle, with respect to the sample surface normal.

TABLE II Surface stress ($\sigma_{11} = \sigma_{22}$) and average of through the thickness normal stress ($\bar{\sigma}_{33}$) in the NiO

Oxidation Temperature, °C	ϕ	$\sigma_{11} = \sigma_{22}$ MPa (psi)	$\bar{\sigma}_{33}$ MPa (psi)
760	0	−167.6 (24,300)	4.8 (700)
	90	−160.0 (−23,200)	13.8 (2,000)
816	0	−186.0 (−27,000)	50.3 (7,300)
	90	−167.5 (−24,300)	33.2 (4,800)
871	0	−183.4 (−26,600)	37.9 (5,500)
	90	−200.6 (−29,100)	46.2 (6,700)
927	0	−213.8 (31,000)	11.7 (1,700)
	90	−233.8 (−33,900)	15.9 (2,300)
982	0	−134.4 (−19,500)	60.0 (8,700)
	90	−93.1 (−13,500)	85.5 (12,400)

Note: These stress values were calculated using an average room temperature Young's Modulus of 1.11×10^5 MPa (16.1×10^6 psi) for NiO (from [22]). A Poisson's ratio of 0.3 was assumed, since data is not available in literature on Poisson's ratio for NiO.

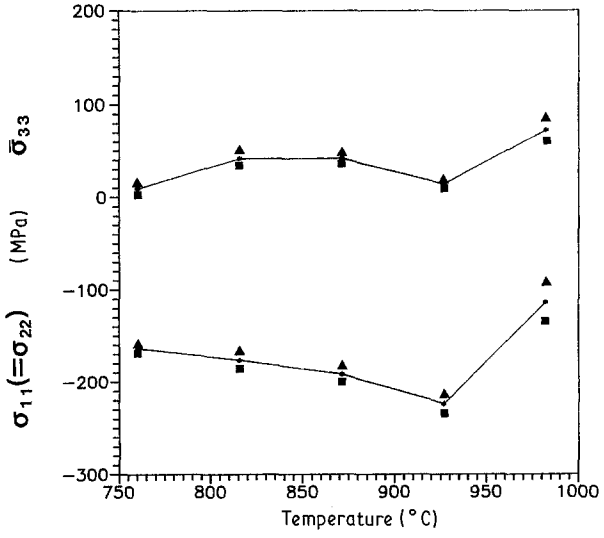

Figure 4 Plot of in-plane $\sigma_{11}(\sigma_{22})$ stresses (compressive) and average normal σ_{33} stresses (tensile) against oxidation temperature (■) $\phi = 0°$, (▲) $\phi = 90°$.

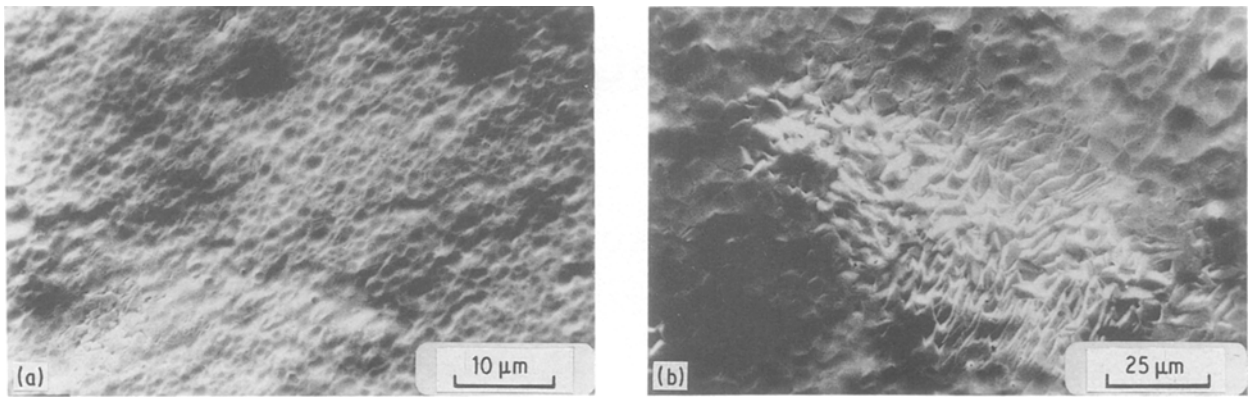

Figure 5 Scanning electron micrographs of samples oxidized at (a) 871° C and (b) 982° C. Equiaxed NiO grains can be seen in (a) and buckled (or extruded) NiO grains can be seen in (b).

5. Conclusion

An X-ray diffraction technique was successfully used to measure oxide scale stresses in NiO formed on Ni200. The in-plane stresses in the oxide scales were found to be compressive and the average normal stresses through the thickness of the scales were found to be tensile. These stresses were found to increase with increasing oxidation temperature up to 927° C. The drop in the in-plane compressive stress in the scale formed at higher temperature was attributed to the stress relaxation due to buckling of the scale.

References

1. N. B. PILLING and R. E. BEDWORTH, *J. Inst. Metals* **29** (1923) 259.
2. D. R. HOLMES and W. H. WHITLOW, Conference on "Mechanical properties and adherence of scale layers and their influence on the oxidation of metals", Dusseldorf, December 1971, *Werkstoffe und Korrosion* **23** (1972) 74.
3. J. V. CATHCART, (ed.), "Stress effects and the oxidation of metals" (TMS-AIME, New York, 1975).
4. D. L. DOUGLASS, *Oxid. Metals* **1** (1969) 127.
5. J. STRINGER, *Corros. Sci.* **10** (1970) 513.
6. *Idem*, *Werkstoffe und Korrosion* **23** (1972) 747.
7. P. HANCOCK and R. C. HURST, in "Advances in corrosion science and technology", edited by M. G. Fontana and R. W. Staehle (Plenum, New York, 1974) p. 1.
8. J. V. CATHCART, in "Properties of high temperature alloys", edited by Z. A. Foroulis and F. S. petit (The Electrochemical Society, Princeton, New Jersey, 1976) p. 99.
9. J. V. CATHCART and R. E. PAWEL, in "Corrosion/erosion of coal conversion system materials", Conference proceedings, Berkeley, California (NACE National Association of Corrosion Engineers), California, 1979).
10. R. E. PAWEL, J. V. CATHCART and J. CAMPBELL, *J. Electrochem. Soc.* **110** (1963) 551.
11. R. E. PAWEL and J. CAMPBELL, *ibid.* **116** (1969) 828.
12. R. E. PAWEL and J. CAMPBELL, *Acta Metall.* **14** (1966) 1827.
13. D. BRUCE and P. HANCOCK, *J. Inst. Metals* **97** (1969) 140.
14. *Idem*, *ibid.* **97** (1969) 148.
15. R. C. HURST and P. HANCOCK, in conference on "Mechanical properties and adherence of scale layers and their influence on the oxidation of metals", Dusseldorf, December 1971, *Werkstoffe und Korrosion* **23** (9) (1972) 773.
16. P. HANCOCK, in "Stress effects and the oxidation of metals," edited by J. V. Cathcart, TMS–AIMG, New York, 1975, p. 155.
17. B. D. CULLITY, "Elements of X-ray diffraction" (Addison Wesley, Mass., USA, 1978) p. 447.
18. ASTM X-ray powder data file No. 4-0835 for NiO and No. 4-0836 for Cu (American Society for Testing and Materials, Philadelphia, Pennsylvania, USA, 1960).
19. P. DOIG and P. E. FLEWITT, *Strain* **13** (1977) 102.
20. I. C. NOYAN, *Metall. Trans.* **14A** (1983) 249.
21. C. J. KELLY and A. M. SHORT, SAE Technical report J784.a (1971) p. 61.
22. "Engineering properties of selected ceramic materials" (American Ceramic Society, Columbus, 1966) Section 5.4.11–4).
23. F. N. RHINES and R. G. CONNELL, in "Properties of high temperature alloys", edited by Z. A. Foroulis and F. J. Petit (Electrochemical Society, Princeton, New Jersey, 1976) p. 154.

Received 18 January
and accepted 1 June 1988